Soliton interaction for a nonlinear discrete double chain

A. Bülow, D. Hennig, and H. Gabriel

Fachbereich Physik, Institut für Theoretische Physik Arnimallee 14, Freie Universität Berlin, 14195 Berlin, Germany
(Received 13 November 1997; revised manuscript received 30 April 1998)

We investigate solution behavior with an emphasis on the localization of a double chain built up from two coupled one-dimensional Ablowitz-Ladik (AL) lattices. Whereas each one-dimensional AL lattice is completely integrable, the AL-type coupling between them causes the system to become nonintegrable. With regard to the stationary system we present a rigorous proof of its nonintegrability by means of the Melnikov method. Concerning stationary localized states, we identify the parameter regions for which the origin of the stationary map represents a hyperbolic equilibrium point. We show the existence of transversal intersections of the stable and unstable manifolds of the hyperbolic point. The associated homoclinic orbit is used to excite standing bright two-soliton-like excitations on the double chain. We compute both, analytically as well as numerically, the dynamical energy exchange rate between the two AL strings when on each of them a single AL soliton is launched. It is shown that the soliton interaction depends on the distance between the solitons and their mutual phase relation. There exist distinct energy exchange regimes ranging from suppressed to pronounced energy exchange. In the latter case directed energy flow from one chain into the other takes place. Eventually almost all energy is stored in a single chain in the form of a breather solution showing a bias toward one-dimensional coherent excitation patterns. In general, the single solitons from the integrable limit with no mutual coupling survive as moving breathers under the action of the nonintegrable coupling, and thus experience no lattice pinning. The only pinned solution we obtained resulted from the homoclinic orbit derived from the stationary system. As an interesting dynamical feature we observe that a single soliton may split into two moving breathing states of different amplitudes as well as different velocities. [S1063-651X(99)07702-8]

PACS number(s): 41.20.Jb, 63.20.Pw, 63.20.Ry

I. INTRODUCTION

Discrete nonlinear lattice systems have attracted considerable interest in the last years [1–25]. By now it is well established that nonlinear lattice systems may exhibit self-localized excitations, e.g., in the form of solitons or breathers, viz. spatially localized and time-periodic solutions. While for exact soliton solutions the integrability of the corresponding lattice system is required, breather solutions are also found in nonintegrable lattice systems. Recently, rigorous results have been obtained concerning the existence and stability of breathers in nonlinear lattices [18,26,27]. Intrinsic localized modes have been observed experimentally in an electric network [28]. Many investigations, mostly of a numerical nature, have been performed to explore the stationary and dynamical properties of self-localized states. However, most studies focused on systems extending in one spatial direction only, while less has been done with respect to lattice systems with more than one spatial dimension. The dynamics of two coupled (1+1)-dimensional nonlinear continuum Schrödinger equations were studied in the context of nonlinear optics, where they describe pulse propagation in birefringet optical fibers [29–32]. Furthermore, in Refs. [33–35] the dynamics of a system consisting of two coupled chains of masses representing a DNA model were investigated.

In the present paper we study a discrete double chain consisting of two coupled one-dimensional Ablowitz-Ladik (AL) lattice strings. Choosing the AL system as the backbone for the double chain was also motivated by the fact, that it realizes a possible discretization of a partial differential equation, namely, the continuum nonlinear Schrödinger (NLS) equation, as a model of significant physical relevance. The latter represents a completely integrable equation, and finds application in numerous physical contexts ranging from optical pulse propagation in nonlinear fibers to condensed matter physics, fluid mechanics, and biophysics. In particular, soliton solutions as self-localized states play an important role. The one-dimensional AL system is also integrable, and supports soliton solutions which are essentially the discrete version of the NLS solitons [36–38]. However, for many physical contexts the 1+1 description is insufficient, and more than one spatial extension has to be taken into account. There is yet another aspect making the study of coupled AL systems worthwhile, namely, the question of whether integrability is provided only in the one-dimensional case. In other words: Do coupled AL systems maintain integrability and exhibit self-localized states in the form of solitons? We know from the inverse scattering transformation that the solutions of one-dimensional AL systems do not interact in nonlinear spectral space [36,37]. Therefore, coupled AL systems offer a possibility to address the issue of *soliton interaction*, for instance in the situation when either chain is initiated with an exact AL soliton.

In the current paper we undertake a detailed discussion of the stationary and dynamical properties of the AL double chain with an emphasis on the excitation of localized solutions. In Sec. II we introduce the model of the double chain. An investigation of the stationary system is performed in Sec. III. The latter can be formulated in terms of a symplectic four-dimensional map. We study its equilibrium points and their stability properties in Sec. IV. As long as the map

origin represents a hyperbolic equilibrium, the formation of stationary bright solitonlike solutions on the double chain is possible. However, the four-dimensional map is nonintegrable, which is shown rigorously by means of the Melnikov method in Sec. V. We exploit the homoclinic orbit associated with the intersecting stable and unstable manifolds of the unstable map origin to create a *pinned* two-soliton-like state on the double chain. In Sec. VI we study the dynamical energy exchange between the two AL strings, when on each of them an exact AL soliton is launched. We demonstrate that the exact AL solitons sustain weak nonintegrable interchain couplings as *moving* breathers not experiencing a pinning potential.

II. AL DOUBLE CHAIN

We introduce the model of the AL double chain built up from two coupled one-dimensional AL lattice chains (strings), each infinitely extended along the horizontal direction. Vertically opposite sites on the two chains are coupled to each other via the interchain coupling parameter α. The coupling along each chain (horizontal coupling) is governed by the parameter V. The system of coupled equations reads

$$i\frac{\partial \Phi_n}{\partial t} = -V(1+\mu|\Phi_n|^2)(\Phi_{n+1}+\Phi_{n-1})$$
$$-\alpha(1+\mu|\Phi_n|^2)\Psi_n, \tag{1}$$

$$i\frac{\partial \Psi_n}{\partial t} = -V(1+\mu|\Psi_n|^2)(\Psi_{n+1}+\Psi_{n-1})$$
$$-\alpha(1+\mu|\Psi_n|^2)\Phi_n. \tag{2}$$

(The nonlinearity parameter μ can be set to unity due to the scaling property of the AL system.) The corresponding Hamiltonian is determined by

$$H = -V\sum_n \ (\Phi_n\Phi_{n+1}^*+\Phi_n^*\Phi_{n+1})$$

$$-V\sum_n \ (\Psi_n\Psi_{n+1}^*+\Psi_n^*\Psi_{n+1})$$

$$-\alpha\sum_n \ (\Phi_n^*\Psi_n+\Psi_n^*\Phi_n)$$

$$\equiv H_0^{(1)}(\Phi) + H_0^{(2)}(\Psi) + H_{int}(\Phi,\Psi). \tag{3}$$

Using the deformed Poisson brackets [42–44]

$$\{\Phi_n,\Phi_m^*\} = i(1+\mu|\Phi_n|^2)\delta_{n,m}, \tag{4}$$

$$\{\Phi_n,\Phi_m\} = \{\Phi_n^*,\Phi_m^*\} = 0, \tag{5}$$

the equations of motion can be derived from Hamiltonian (3) as

$$\dot{\Phi} = \{H,\Phi\}, \quad \dot{\Psi} = \{H,\Psi\}, \tag{6}$$

yielding the (deformed) canonical equations

$$i\dot{\Phi}_n = \frac{\partial H}{\partial \Phi_n^*}(1+\mu|\Phi_n|^2),$$

$$i\dot{\Psi}_n = \frac{\partial H}{\partial \Psi_n^*}(1+\mu|\Psi_n|^2). \tag{7}$$

With our choice of nonlinear coupling both the horizontal and vertical couplings are of AL type. This symmetric coupling type has to be distinguished from other nonlinear couplings arising in the optical fiber models [29–32]. Note that for vanishing horizontal couplings $V=0$ the system of equations (1) and (2) decouples into integrable AL dimers, whereas for zero vertical couplings $\alpha=0$ it decomposes into two one-dimensional integrable AL chains. The one-dimensional AL lattice is completely integrable [36–38], and exhibits soliton solutions. These solitons can travel along the lattice chain keeping their form invariant. (For studies of problems related with the AL equation, see Refs. [38–46].) On the other hand, we know that most nonlinear lattice systems are nonintegrable. For illustration we consider the one-dimensional AL lattice corresponding to Eq. (1) in the absence of the coupling term, i.e. $\alpha=0$. Adding then for instance a local cubic nonlinear term $\gamma|\Phi_n(t)|^2\Phi_n(t)$ to the right-hand side (rhs) of Eq. (1) renders this one-dimensional generalized discrete nonlinear Schrödinger (GDNLS) equation into a nonintegrable system [42,44,47]. Due to the nonintegrability, exact soliton solutions are no longer supported. When launching an AL soliton on the GDNLS lattice one observes that it may become pinned under the influence of the periodic lattice potential [9,44,47], preventing solitary waves from propagating along the GDNLS lattice. Since the AL double chain consists of two integrable AL strings also coupled through an AL term, the interesting question arises of whether the coupled system of Eqs. (1) and (2) is still integrable and has soliton solutions. Perturbational methods become applicable in the case of weak couplings. We use the case of weak interchain couplings for which α is taken to be small compared to the horizontal coupling strength V.

Remarkably, the associated stationary system of the coupled AL double chain is nonintegrable, which is demonstrated rigorously further below (see Sec. V). In connection with the nonintegrable stationary map the existence of homoclinic orbits can be shown. Taking the points of the latter as the initial condition for the time-dependent system, a *standing* localized solitonlike solutions on the AL double chain is excited. As will be shown, for each parameter set there is one and only one set of initial conditions leading to such an exact standing localized eigenstate. On the other hand, the dynamical solitons of the one-dimensional AL systems generally ''survive'' as breathing solitonlike excitations *moving* along the two AL strings.

III. STATIONARY SYSTEM

We are interested in stationary solutions of the system of equations (1) and (2) and make the ansatz

$$\Psi_n(t)=a_n e^{-i\omega t}, \quad \Phi_n=b_n e^{-i\omega t}, \quad (8)$$

with a uniform rotation frequency ω. In Ref. [47] it was shown that to obtain localized solutions one has to rely on real-valued amplitudes $a_n, b_n \in R$. Substituting Eq. (8) into Eqs. (1) and (2) we arrive at two coupled second-order difference equations

$$\omega a_n = -V(1+\mu a_n^2)(a_{n+1}+a_{n-1})-\alpha b_n(1+\mu a_n^2), \quad (9)$$

$$\omega b_n = -V(1+\mu b_n^2)(b_{n+1}+b_{n-1})-\alpha a_n(1+\mu b_n^2). \quad (10)$$

(For the sake of simplicity we set $V\equiv1$ in the following.) With the help of the substitutions

$$a_n=x_n, \quad a_{n-1}=y_n, \quad b_n=u_n, \quad b_{n-1}=v_n, \quad (11)$$

we cast the difference system of equations (9) and (10) into a four-dimensional map A: $R^4 \rightarrow R^4$ obeying the iteration rules

$$\vec{x}_{n+1}=\mathcal{A}\vec{x}_n^T, \quad (12)$$

with the amplitude vector

$$\vec{x}_n=(x_n,u_n,y_n,v_n)\in R^4 \quad (13)$$

and the matrix

$$\mathcal{A}=\begin{pmatrix} -\dfrac{\omega}{1+\mu x_n^2} & -\alpha & -1 & 0 \\[2mm] -\alpha & -\dfrac{\omega}{1+\mu u_n^2} & 0 & -1 \\[2mm] 1 & 0 & 0 & 0 \\[1mm] 0 & 1 & 0 & 0 \end{pmatrix}. \quad (14)$$

The map A is initiated with the starting values (x_1,u_1,y_1,v_1) corresponding to the two pairs of stationary amplitudes $(a_{0,1},b_{0,1})$, e.g., at the left ends of the two chains, respectively. With each forward iteration step of the map A^{n+1}, one generates the amplitudes a_{n+1} and b_{n+1} at sites that are the neighbors to the right of those of the preceding step A^n. Conversely, iterating the inverse map A^{-1} generates amplitude patterns to the left of the starting sites. The map A is volume preserving because the condition $\det(DA)=1$ is fulfilled for all vectors $\vec{x}$, and DA is the Jacobi matrix of A.

Being interested in the excitation of localized states on the double chain, we recall that such localized stationary lattice solutions correspond to map orbits lying on the stable and unstable manifolds of hyperbolic equilibria [47]. Therefore, Sec. IV deals with an analysis of the equilibrium positions of the map A. In particular, we locate the fixed points of A and investigate their stability and bifurcation behavior.

Taking the limit $\alpha=0$ the four-dimensional map A is equivalent to a pair of two-dimensional AL maps, each corresponding to a stationary one-dimensional AL lattice. For $\omega<-2$ the origin of such a two-dimensional map represents an unstable hyperbolic point [47]. The coinciding stable and unstable manifolds of the hyperbolic point at (0,0) form a perfect separatrix which is manifested as a standing bright soliton on the (one-dimensional) AL lattice. (For the integrable one-dimensional AL lattice such a standing soliton can be moved with any desired velocity through a Galileo boost [37].) When both two-dimensional AL maps become coupled for $\alpha>0$, it is of particular interest which of the parameters that sets the origin is a hyperbolic equilibrium. Orbits on its invariant stable and unstable manifolds still support stationary solitonlike solutions of the coupled AL double chain. Finally, we remark that the symplecticity of the map A is a readily proven property helpful for a stability analysis of periodic orbits.

IV. EQUILIBRIUM POSITIONS AND LINEAR STABILITY ANALYSIS

We investigate the equilibrium positions of A and their corresponding stability properties. The map A possesses periodic points of order k if the condition

$$\mathcal{A}^k\vec{x}_F=\vec{x}_F, \quad k\in N \quad (15)$$

holds and the points $\vec{x}_F$ determine a periodic orbit. To determine the stability of such orbits we make use of the fact that for symplectic maps linear stability implies spectral stability. (A periodic orbit is linearly stable if all small perturbations of it remain bounded for the evolution of the tangent map. Spectral stability means that all eigenvalues of the tangent map lie on the unit circle, i.e., $|\lambda|=1$ [48,49].) The eigenvalues λ of the tangent map are determined by the characteristic polynomial

$$\det(DA-\lambda I)=0, \quad (16)$$

and the Jacobian matrix is given by

$$(DA)=\begin{pmatrix} p(x) & -\alpha & -1 & 0 \\ -\alpha & p(u) & 0 & -1 \\ 1 & 0 & 0 & 0 \\ 0 & 1 & 0 & 0 \end{pmatrix}, \quad (17)$$

with

$$p(x)=\frac{-\mu\omega x_n^2+1\,\omega}{(1+\mu x_n^2)^2}, \quad (18)$$

$$p(u)=\frac{-\mu\omega u_n^2+1\,\omega}{(1+\mu u_n^2)^2}. \quad (19)$$

Due to the symplectic property of the map, $1/\lambda$ is also an eigenvalue. If $|\lambda|\neq1$ and $\text{Im}(\lambda)\neq0$ the eigenvalues appear as symmetric 4-tuples: λ, λ^*, $1/\lambda$, $1/\lambda^*$. If $\text{Im}(\lambda)=0$, then a pair λ, $1/\lambda$ exists on the real axis and the orbit is

unstable. Finally, if $|\lambda|=1$ then there is a pair λ, $\lambda^*=1/\lambda$, and the orbit is stable. The characteristic polynomial corresponding to the tangent map DA is

$$\det(DA-I\lambda)=P(\lambda)=\lambda^4-K\lambda^3+L\lambda^2-K\lambda+1=0, \tag{20}$$

with

$$K=\text{Tr}(DA) \quad \text{and} \quad L=\frac{[\text{Tr}(DA)]^2-\text{Tr}(DA)^2}{2}. \tag{21}$$

$\text{Tr}(DA)$ is the trace of the tangent map. Using Eqs. (18) and (19), the coefficients K and L are given by

$$K=p_x+p_u \quad \text{and} \quad L=p_xp_u-\alpha^2+2. \tag{22}$$

Instead of studying the quartic characteristic polynomial, it is more convenient to investigate the reduced characteristic polynomial that is quadratic in the stability index $\rho=\lambda+1/\lambda$:

$$Q(\rho)=\rho^2-K\rho+L-2=0. \tag{23}$$

The solutions

$$\rho_{1,2}=\tfrac{1}{2}K\pm\sqrt{\tfrac{1}{4}K^2-L+2} \tag{24}$$

are related to ρ by

$$\lambda_{1,2}=\frac{\rho\pm\sqrt{\rho^2-4}}{2}. \tag{25}$$

Since stability requires the eigenvalues to lie on the unit circle, i.e., $|\lambda|=1$, the inequality

$$|\rho|\leq 2 \tag{26}$$

must hold. Using Eq. (21), the stability indices are determined by

$$\rho_{1,2}=\frac{p_x+p_u}{2}\pm\sqrt{\frac{p_x^2+p_u^2}{4}-\frac{p_xp_u}{2}+\alpha^2}. \tag{27}$$

Finally, according to Eq. (25) the four eigenvalues of the tangent map DA are given by

$$\lambda_{1,2}=\frac{1}{4}\left\{p_x+p_u+\sqrt{z}\pm2\sqrt{-4+\left(-\frac{p_x+p_u-\sqrt{z}}{2}\right)^2}\right\}, \tag{28}$$

$$\lambda_{3,4}=\frac{1}{4}\left\{p_x+p_u-\sqrt{z}\pm2\sqrt{-4+\left(-\frac{p_x+p_u+\sqrt{z}}{2}\right)^2}\right\}, \tag{29}$$

with

$$z=4\alpha^2+p_u^2+p_x^2-2p_up_x. \tag{30}$$

The eigenvalues depend on the coordinates of the periodic orbit $\vec{x}_F$ as well as on the system parameters, that is, $\lambda_{1,2,3,4}=\lambda_{1,2,3,4}(\vec{x}_F;\alpha,\omega)$. The parameter range in which the equilibria of the map A are stable can be determined from $|\lambda(\vec{x}_F,\alpha,\omega)|=1$. However, upon parameter variations bifurcations may occur for which the stability can alter [49,50]. With regard to the stability loss of a stable fixed point of the double AL chain, we distinguish two possible situations depending on how the eigenvalues move away from the unit circle as parameters are changed.

(i) A pair of complex conjugate eigenvalues encounters at the point (1,0) and separates along the positive real axis. This so-called tangent bifurcation occurs for

$$L<2K-2, \tag{31}$$

and gives the condition

$$\alpha>\pm\sqrt{-2(p_x+p_u)+p_xp_u+4} \tag{32}$$

for the coupling parameter α.

(ii) A pair of complex conjugate eigenvalues moves to $(-1,0)$ and separates along the negative real axis which is called period doubling bifurcation. This happens when

$$L<-2K-2, \tag{33}$$

which is fulfilled if

$$\alpha>\pm\sqrt{2(p_x+p_u)+p_xp_u+4}. \tag{34}$$

The task now is to locate the periodic orbits of A and to determine their stability properties. We focus interest on period-1 orbits, viz. fixed points. Inserting $\vec{x}_F=(x_F,u_F,y_F,v_F)$ in Eq. (15) results, for $k=1$, in the coupled system

$$2x_F=-\frac{\omega}{1+\mu x_F^2}x_F-\alpha u_F,$$

$$\tag{35}$$

$$2u_F=-\frac{\omega}{1+\mu u_F^2}u_F-\alpha x_F.$$

This can be solved for x_F to give
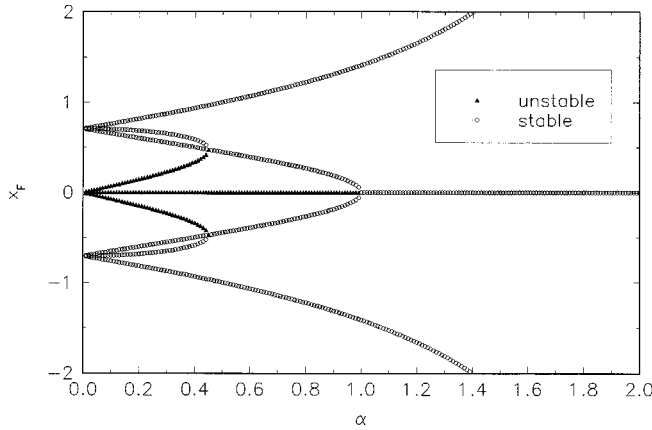
FIG. 1. Location of the fixed points x_F vs α. Parameters $\omega = -3$, $\mu = 1$, and $V = 1$. Stability as indicated.

$$0 = \alpha x_F + \frac{\mu x_F^3 (2 + \omega + 2\mu x_F^2)^2}{\alpha(1 + \mu x_F^2)^2} - \frac{2\mu x_F^3 (2 + \omega + 2\mu x_F^2)^3}{\alpha^3 (1 + \mu x_F^2)^3}$$

$$- \frac{(2 + \omega) x_F (2 + \omega + 2\mu x_F^2)}{\alpha(1 + \mu x_F^2)}$$

$$= P(x_F).$$

The roots of this polynomial $P(x_F)$ yield the location of the fixed points of A. We immediately see that $\vec{x}_F = \vec{0}$ is always a fixed point. The remaining roots of $P(x_F)$ can be found numerically with the help of a Newton procedure. The number of roots (fixed points) ranges from one up to nine depending on the parameter values. Figure 1 shows the location x_F of the fixed point versus the coupling parameter α for $\omega = -3$. For $\alpha < 0.46$ there exist nine fixed points. Their number diminishes to five for $\alpha > 4.6$. A further reduction occurs at $\alpha = 1$, and three stable equilibria survive. Eventually, for $\alpha > 1.4$, only one stable elliptic fixed point at the origin remains. In the context of the present paper—that is, to study solitonlike solutions—the stability property of the fixed point at the origin deserves closer inspection. As long as the latter is of hyperbolic stability type, the orbits on its associated invariant stable and unstable manifolds support bright solitonlike lattice solutions (also see Sec. V).

The eigenvalues of the tangent map at $(0,0,0,0)$ are given by

$$\lambda_{1,2} = \tfrac{1}{2}(\omega + \alpha \pm \sqrt{(\alpha - \omega)^2 - 4}), \tag{36}$$

$$\lambda_{3,4} = \tfrac{1}{2}(\omega - \alpha \pm \sqrt{(\alpha - \omega)^2 - 4}), \tag{37}$$

and depend on the parameters ω and α. We determine the border lines for stability in the $\omega - \alpha -$ parameter plane as follows.

If

$$\alpha > \sqrt{\omega^2 + 4\omega + 4} \quad \text{and} \quad \alpha > \sqrt{\omega^2 - 4\omega + 4} \tag{38}$$

hold, the fixed point is unstable.

If

$$\alpha < \sqrt{\omega^2 + 4\omega + 4} \quad \text{and} \quad \alpha < \sqrt{\omega^2 - 4\omega + 4}, \tag{39}$$

the range in which the fixed point is elliptic is given by

$$|\omega \pm \alpha| \leq 2. \tag{40}$$

A hyperbolic point exists if

$$|\omega \pm \alpha| > 2. \tag{41}$$

If

$$\alpha < \sqrt{\omega^2 - 4\omega + 4}, \quad \alpha > \sqrt{\omega^2 + 4\omega + 4}, \quad \text{and} \quad |\omega + \alpha| \leq 2 \tag{42}$$

are satisfied, the fixed point is elliptic.

For $\alpha > 1$ the origin is converted into a stable elliptic fixed point. In this case, when vertical coupling and horizontal coupling exceeds $((\alpha/V) > 1)$, the excitation of bright solitonlike solutions on the AL strings is impossible due to the lack of a hyperbolic point at $(0,0,0,0)$.

Figures 2(a) and 2(b) illustrate the complex behavior of the map A, the orbits of which are projected on the x-y subplane. For comparison, Fig. 2(a) displays the integrable two-dimensional AL map of $\alpha = 0$ for $\omega = -3$ and $V = 1$. The perfect separatrix associated with the hyperbolic point at the origin yields a stationary soliton on the AL lattice. For $\alpha > 0$ this separatrix is broken and is surrounded by a chaotic layer [see Fig. 3(b)]. The u-v subplane shows a similar feature of nonintegrable map dynamics.

V. NONINTEGRABILITY OF THE STATIONARY AL DOUBLE CHAIN AND MELNIKOV ANALYSIS

In this section we apply the Melnikov method to show rigorously the nonintegrability of the stationary AL double chain. The Melnikov method represents an analytical tool to prove transversal intersections of manifolds invariant to hyperbolic equilibria [49–52]. It applies to maps of the form

$$\vec{x}_{n+1} = A\vec{x}_n = F\vec{x}_n + \epsilon G\vec{x}_n, \tag{43}$$

where A is decomposed into an integrable part F and a weak perturbational part G, with $\epsilon \ll 1$ regulating the strength of the perturbation. The integrable map F possesses a hyperbolic equilibrium point located at the origin. The stable and unstable manifolds of this hyperbolic point coincide forming a separatrix on which the solution is known explicitly.

For the four-dimensional coupled AL map $\vec{x}_{n+1} = F\vec{x}_n + \alpha G\vec{x}_n$, the integrable part is determined by

$$F(\vec{x}_n) = \begin{pmatrix} \dfrac{-\omega x_n}{1 + \mu x_n^2} - y_n \\[2ex] \dfrac{-\omega u_n}{1 + \mu u_n^2} - u_n \\[2ex] x_n \\[1ex] u_n \end{pmatrix}, \tag{44}$$

and the nonintegrable perturbation arising from the (weak) interchain coupling reads as

(a)

(b)
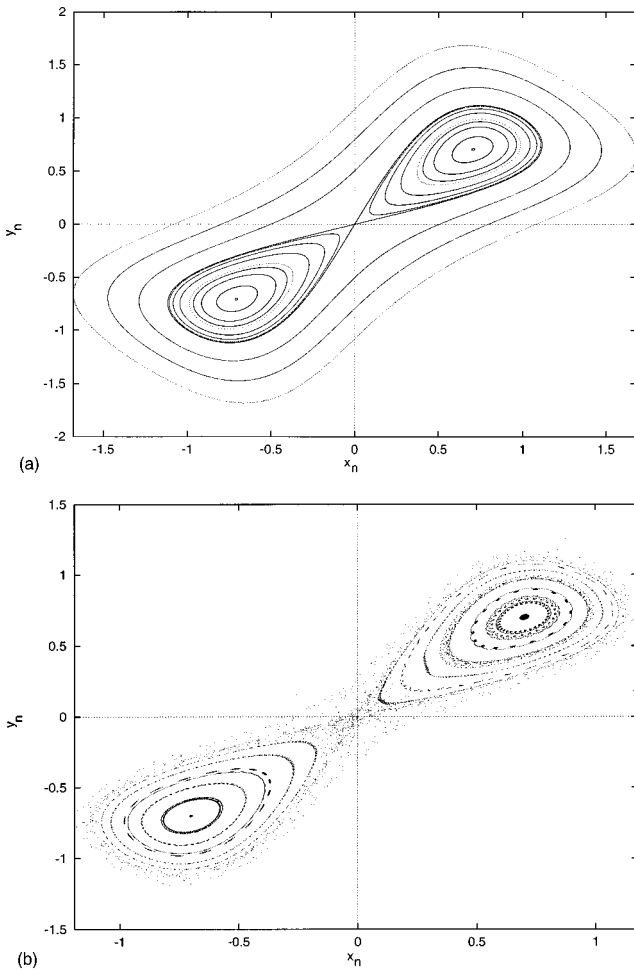
FIG. 2. Orbits of the map A given in Eqs. (12) projected on the x-y subplane for the following parameters: (a) No interchain coupling $\alpha = 0$. The integrable two-dimensional AL map. Note the perfect separatrix. (b) Interchain coupling $\alpha = 0.1$. The separatrix is broken due to nonintegrability of the map A.

$$G(\vec{x}_n) = - \begin{pmatrix} u_n \\ x_n \\ 0 \\ 0 \end{pmatrix}. \tag{45}$$

The map origin represents a hyperbolic fixed point for $\omega < -2$. The corresponding unperturbed homoclinic orbit for $\alpha = 0$ is parametrized by

$$\vec{x}_n^{\,0}(s,t) = \frac{1}{\sqrt{\mu}} \sinh(\beta) \begin{pmatrix} \mathrm{sech}(t - n\beta) \\ \mathrm{sech}(s - n\beta) \\ \mathrm{sech}(t - (n+1)\beta) \\ \mathrm{sech}(s - (n+1)\beta) \end{pmatrix} \in R^4, \tag{46}$$
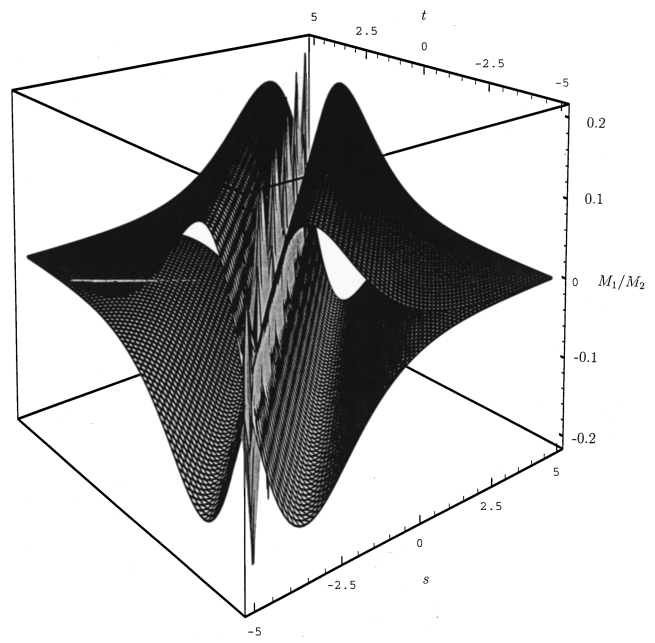
FIG. 3. Amplitudes $M_{1,2}$ of the two components of the Melnikov vector vs the separatrix parameters s and t. The values on the line $s = t$ have been scaled by a factor 100.

and consists of the two two-dimensional separatrices assigned to the upper and lower AL strings. The connection between β and ω is given by

$$\cosh\beta = -\frac{\omega}{2}. \tag{47}$$

The parameter s (t) determines the position on the separatrix of the integrable upper (lower) AL string, and hence the lattice position of the soliton on the corresponding one-dimensional lattice. (In Sec. VI the parameters $s = x_0$ and $t = y_0$ are used to fix the initial lattice positions of the moving solitons.) The question now is: How does string coupling $\alpha > 0$ affect these single solitons on each of the two AL strings?

As is well known under nonintegrable perturbations, the stable and unstable manifolds invariant to the hyperbolic point are no longer identical and rather may intersect each other transversally, thus forming a homoclinic tangle [49,50]. Based on geometrical arguments, a Melnikov function was developed measuring for nonintegrable planar maps ($N = 2$) the distance between the stable and unstable manifold under the action of perturbations [52]. Using analytical techniques developed in Refs. [53,54], the Melnikov method has been extended to treat maps with dimensions $N \geq 2$ as well [53–56], and the (scalar) Melnikov function is replaced by a Melnikov vector of N components related to the gradients of the integrals of the unperturbed system. The components of the Melnikov vector are defined by

$$M_i(s,t) = \alpha \sum_{n=-\infty}^{\infty} \vec{\tilde{q}}_{n+1}^{\,(i)} G(\vec{x}_n^{\,0}(s,t)), \quad i = 1,2. \tag{48}$$

Isolated zeros (s^*,t^*) of the components exist for

$$M_i(s^*,t^*)=0, \qquad (49)$$

$$\det D\vec{M}\neq 0, \qquad (50)$$

implying the existence of transversal intersections of the invariant manifolds yielding homoclinic orbits. (For details, see Ref. [56].)

To derive the vector $\tilde{\vec{q}}_{n+1}^{(i)}$ appearing in Eq. (48), we first have to solve a variational problem [56] associated with the unperturbed system:

$$\vec{q}_{n+1}=D_n\vec{q}_n. \qquad (51)$$

D_n is the Jacobi matrix $D_n=DF(\vec{x}_n^0)$. The adjoint variational problem then provides $\tilde{\vec{q}}_{n+1}$:

$$\tilde{\vec{q}}_{n+1}=\tilde{\vec{q}}_n D_n^{-1}. \qquad (52)$$

It is possible to calculate the components of the vectors $\vec{q}_n^{(1)}$ and $\vec{q}_n^{(2)}$ through the partial derivatives of the separatrix expression $(\vec{x}_n^0(t,s))$ taken with respect to its separatrix parameters s and t:

$$\vec{q}_n^{(1)}=\frac{\partial\vec{x}_n^0(t,s)}{\partial t}, \quad \vec{q}_n^{(2)}=\frac{\partial\vec{x}_n^0(t,s)}{\partial s}. \qquad (53)$$

The results are

$$\vec{q}_n^{(1)}(t)=\frac{1}{\sqrt{\mu}}\begin{pmatrix} \text{sech}(\beta n-t) & \tanh(\beta n-t) \\ 0 & \\ \text{sech}(\beta(n+1)-t) & \tanh(\beta(n+1)-t) \\ 0 & \end{pmatrix}, \qquad (54)$$

$$\vec{q}_n^{(2)}(s)=\frac{1}{\sqrt{\mu}}\begin{pmatrix} 0 & \\ \text{sech}(\beta n-s) & \tanh(\beta n-s) \\ 0 & \\ \text{sech}(\beta(n+1)-s) & \tanh(\beta(n+1)-s) \end{pmatrix}. \qquad (55)$$

For the ease of notation we introduce the abbreviations

$$S_n(t)=\text{sech}(n\beta-t), \quad T_n(t)=\tanh(n\beta-t), \qquad (56)$$

$$C=\frac{1}{\sqrt{\mu}}\sinh\beta. \qquad (57)$$

The vectors $\vec{q}_n^{(i)}$ thus take the following forms

$$\vec{q}_n^{(1)}(t)=C(S_n(t),T_n(t),0,S_{n+1}(t),T_{n+1}(t),0), \qquad (58)$$

$$\vec{q}_n^{(2)}(s)=C(0,S_n(s),T_n(s),0,S_{n+1}(s),T_{n+1}(s)). \qquad (59)$$

The vectors $\tilde{\vec{q}}_{n+1}^{(i)}$ demanded for the computation of the Melnikov vector are obtained via the adjoint variational equation [53,56]:

$$\tilde{\vec{q}}_{n+1}^{(i)}=\tilde{\vec{q}}_n^{(i)}\cdot[DF(\vec{x}_n^0)]^{-1} \qquad (60)$$

$$=\tilde{\vec{q}}_n^{(i)}\cdot D_n^{-1}. \qquad (61)$$

We then find

$$\tilde{\vec{q}}_{n+1}^{(1)}=C(S_n(t)T_n(t),0,S_{n+1}(t)T_{n+1}(t)-p_xS_n(t)T_n(t),0) \qquad (62)$$

and

$$\tilde{\vec{q}}_{n+1}^{(2)}=C(0,S_n(s)T_n(s),0,S_{n+1}(s)T_{n+1}(s) \\ -p_uS_n(s)T_n(s)). \qquad (63)$$

The perturbation vector $G(\vec{x}_n^0(t,s))$ can be presented as

$$G(\vec{x}_n^0(t,s))=-C(S_n(s),S_n(t),0,0). \qquad (64)$$

Finally, the components of the Melnikov vector $\vec{M}=(M_1,M_2)$ are given by

$$M_1(t,s)=\alpha\sum_{n=-\infty}^{\infty}\tilde{\vec{q}}_{n+1}^{(1)}G(\vec{x}_n^0(t,s))$$

$$=-\alpha C^2\sum_{n=-\infty}^{\infty}S_n(s)S_n(t)T_n(t), \qquad (65)$$

and correspondingly

$$M_2=\alpha\sum_{n=-\infty}^{\infty}\tilde{\vec{q}}_{n+1}^{(2)}G(\vec{x}_n^0(t,s))$$

$$=-\alpha C^2\sum_{n=-\infty}^{\infty}S_n(s)S_n(t)T_n(t). \qquad (66)$$

The computation of the sums in Eqs. (65) and (66) proceeds along the lines given in Refs. [47,52]. After some lengthy computations the M_1 component of the Melnikov vector for $s\neq t$ is obtained as

$$M_1 = -\alpha \frac{2}{\mu\beta} \sinh^2\beta \left\{ \cosech(s-t) \left(\coth(s-t) \left[\frac{2EK(t-s)}{\beta} + KE\left(am\left[\frac{2Ks}{\beta} \right] \right) \right] - (t-s) - KE\left(am\left[\frac{2Kt}{\beta} \right] \right) \right] \right) \right.$$
$$\left. - \frac{2K^2}{\beta} dn^2\left(\frac{2Kt}{\beta} \right) + \frac{2KE}{\beta} - 1 \right) \right\}. \tag{67}$$

The second component is simply given by

$$M_2 = -M_1. \tag{68}$$

K and E are the complete elliptic integrals of the second kind, and am is a Jacobian elliptic function [57]. The modulus of these functions is defined by

$$q = \exp(-z) = \exp\left(-\pi \frac{K'(k)}{K(k)} \right). \tag{69}$$

For $s=t$ the two-component Melnikov vector reduces to a scalar function $M_1 = M_2 \equiv M_{\text{sym}}$, explicitly given by

$$M_{\text{sym}} = -\alpha C^2 \frac{\partial}{\partial t} \Sigma(t,t,\beta)$$

$$= -\alpha C^2 \frac{16K^3 m}{\beta^3} cn\left(\frac{2Kt}{\beta} \right) dn\left(\frac{2Kt}{\beta} \right) sn\left(\frac{2Kt}{\beta} \right). \tag{70}$$

In Fig. 3 we plot the amplitudes of the two components $M_{1,2}$ of the Melnikov vector as a function of the two separatrix parameters s and t. We recall that the latter determine the positions on the unperturbed separatrix (46) and thus the position of the unperturbed single soliton on each of the two AL strings. To be distinguishable, the values of Eq. (70) (valid on the line $s=t$) have been scaled by a factor of 100. We recognize the following features.
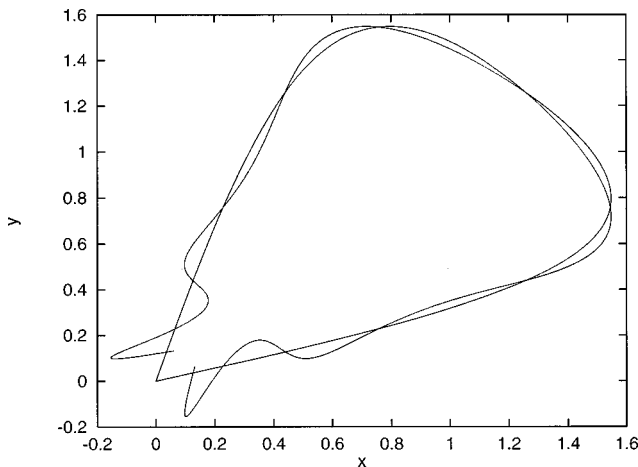
FIG. 4. First windings of the homoclinic tangle of the hyperbolic equilibrium point at (0,0,0,0) for the map A. Parameters: $\omega = -4$, $\mu = 1$, $V = 1$, and $\alpha = 0.2$.

(i) For values of s and t very distant from the line $s=t$ the Melnikov vector is (almost) identically zero, excluding isolated zeros of $M_{1,2}$. Moreover, for $s \neq t$ the components M_1 and M_2 have no common simple zeros and thus no transversal intersections of the invariant manifolds can be detected (at least to first-order perturbational computation of the Melnikov vector considered here).

(ii) Condition (48) can be satisfied only on the line $s=t$. Simple zeros of the Melnikov function M_{sym} occur. The corresponding homoclinic tangling on the x-y plane is depicted in Fig. 4.

Based on the results for the Melnikov analysis we conclude that, only for symmetric excitation of the AL double chain, i.e., for opposite solitons of equal positions $s=t$, the existence of homoclinic chaos in the four-dimensional map is proven. As a consequence both single solitons become pinned. Their lattice amplitudes are determined by the transversal intersection points of the invariant manifolds of the hyperbolic equilibrium (0,0,0,0) on the map A. Such a stationary amplitude profile $|\Phi_n(t)|^2$ of the stationary soliton-like excitation on the upper string is shown in Fig. 5. The lower string exhibits an equal excitation pattern. We computed the energy $H_{\text{pinned}} = -\Sigma_n(\Phi_n\Phi_{n+1}^* + \Phi_n^*\Phi_{n+1}) - (\alpha/2)\Sigma_n|\Phi_n|^2$ of the pinned soliton on the upper string. A comparison showed that the energy of the single stationary AL soliton given by $H_{\text{soliton}} = -4 \sinh\beta$ lies above the pinned state energies. The energy difference $\Delta H = H_{\text{pinned}} - H_{\text{soliton}}$ may be interpreted as the pinning energy of the AL double chain due to its nonintegrability feature.

On the other hand, for unequal soliton positions $s \neq t$ homoclinic chaos cannot be proven. Nevertheless, as the dynamical studies reveal, the AL double chain appears to be nonintegrable (see Sec. VI). Note that the case of symmetric soliton excitation of $s=t$ with its established homoclinic
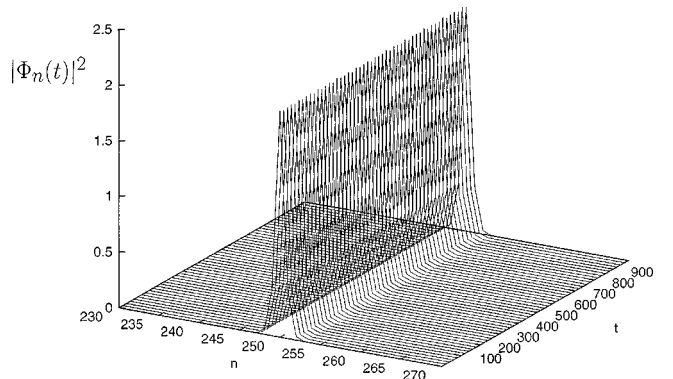
FIG. 5. The amplitude profile of the stationary bright solitonlike solution on the upper string. The homoclinic orbit of the map A has been used as the initial conditions for system (71). Parameters: $\omega = -3$, $V = 1$, $\mu = 1$, and $\alpha = 0.1$.

chaos allows for a construction method of standing solitons being opposite on the AL double chain. Since opposite solitons imply identical initial conditions $\Phi_n(0) = \Psi_n(0)$ the AL double chain degenerates to two one-dimensional GDNLS equations

$$i\frac{\partial \Phi_n}{\partial t} = -V(1+\mu|\Phi_n|^2)(\Phi_{n+1}+\Phi_{n-1})$$
$$-\alpha(1+\mu|\Phi_n|^2)\Phi_n \qquad (71)$$

$$i\frac{\partial \Psi_n}{\partial t} = -V(1+\mu|\Psi_n|^2)(\Psi_{n+1}+\Psi_{n-1})$$
$$-\alpha(1+\mu|\Psi_n|^2)\Psi_n, \qquad (72)$$

the soliton construction proceeds as described in Ref. [47] by exploiting the knowledge on the homoclinic orbit. We sketch the procedure in the following flow diagram.

$$\boxed{\text{system of coupled time-dependent lattice equations}}$$
$$\Downarrow$$
$$\boxed{\text{stationary system}}$$
$$\Downarrow$$
$$\boxed{\text{two-dimensional map}}$$
$$\Downarrow$$
$$\boxed{\text{hyperbolic equilibrium of the map}}$$
$$\Downarrow$$
$$\boxed{\text{Transversal intersections of the stable and unstable manifolds}}$$
$$\Downarrow$$
$$\boxed{\text{corresponding homoclinic orbit} \rightarrow \text{initial conditions for time-dependent system}}$$
$$\Downarrow$$
$$\boxed{\text{exact nonlinear eigenstate}}$$
$$\Downarrow$$
$$\boxed{\text{localization on AL double chain}}$$
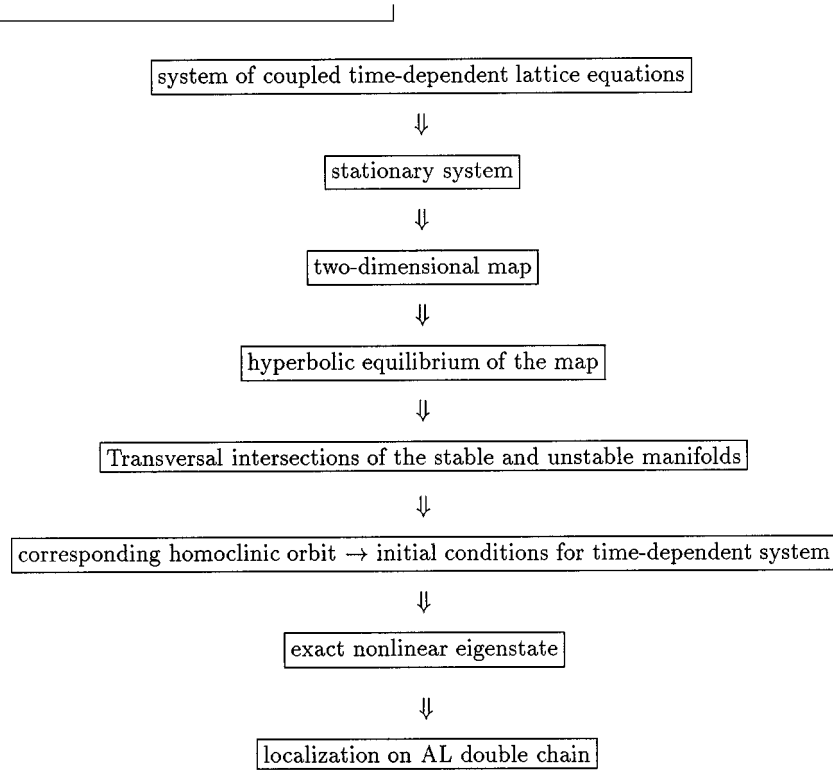
In conclusion, excitation of an exact two-soliton stationary state of the AL double chain is only possible for opposite ($s = t$) single solitons. Finally, in the extreme case of very distant soliton positions s and t, the (stationary) solitons do not affect each other and significant ''soliton interaction'' should not appear (see Sec. VI).

We close this section by emphasizing that the Melnikov analysis is not restricted to an AL double chain of two vertically coupled strings. It rather applies to a (genuine) *two-dimensional stationary AL array* extended arbitrarily both in the longitudinal and vertical directions such that each array site is coupled to its left, right, lower, and upper neighbors. In this sense we are able to prove rigorously the nonintegrability of a stationary two-dimensional AL array.

VI. ENERGY EXCHANGE BETWEEN THE TWO AL STRINGS

In this section we investigate the energy exchange between the two strings of the AL double chain. The findings of Sec. V indicate that the AL double chain is nonintegrable, preventing the system from exhibiting exact soliton states. Nonetheless, for weak interchain coupling we can address the issue of soliton interaction. On each string an exact single AL soliton is excited and the two chains are weakly coupled, i.e., $\alpha \ll 1$. The change of energy of the upper string is determined by

$$\frac{dH_0^{(1)}}{dt} = \alpha\{H_0^{(1)}, H_{\text{int}}\}, \qquad (73)$$

giving, with Eqs. (3) and (5),

$$\frac{dH_0^{(1)}}{dt} = i\alpha \sum_n \ (1+\mu|\Phi_n|^2)[(\Phi_{n+1}^*+\Phi_{n-1}^*)\Psi_n-(\Phi_{n+1}+\Phi_{n-1})\Psi_n^*]$$

$$= -2\alpha\sum_n \ (1+\mu|\Phi_n|^2)\mathrm{Im}[(\Phi_{n+1}^*+\Phi_{n-1}^*)\Psi_n]. \tag{74}$$

An equivalent expression is derived for the change of energy of the lower chain. Since for small couplings of $\alpha\lesssim 0.1$ the ratio $|H_{\mathrm{int}}/H_0^{(1,2)}|$ is less than 10^{-1}, we neglect the contribution from the interaction part H_1 for the energy balance. The change in energy of the second string follows directly from the one of the first string due to energy conservation. The energy exchange rate per time unit T is given by

$$\Delta H_0^{(1)} = -2\alpha\frac{1}{T}\int_T dt\sum_n \ (1+\mu|\Phi_n|^2)\ \mathrm{Im}[(\Phi_{n+1}^*+\Phi_{n-1}^*)\Psi_n]. \tag{75}$$

The (unperturbed) one-soliton solutions on the two strings read as

$$\Phi_n(t) = \frac{\sinh\beta}{\sqrt{\mu}}\mathrm{sech}[\beta(n-ut-x_0)]\exp[-i(\omega t-\theta n+\sigma_0)] \tag{76}$$

$$\Psi_n(t) = \frac{\sinh\beta}{\sqrt{\mu}}\mathrm{sech}[\beta(n-ut-y_0)]\exp[-i(\omega t-\theta n+\delta_0)] \tag{77}$$

$$\omega = -2\cos\theta\cosh\beta, \quad u = \beta^{-1}\sin\theta\sinh\beta, \tag{78}$$

where $\beta\in[0,\infty)$ and $\theta\in[-\pi,\pi]$. Both solitons have equal parameters except for possibly different phases σ_0 and δ_0 as well as soliton positions x_0 on the upper string and y_0 on the lower string. (Note that for the stationary analysis of Sec. V we used the separatrix parameters s and t to determine the positions of the standing solitons.)

For the energy exchange rate we obtain

$$\Delta H_0^{(1)} = -4\alpha\frac{\sinh^2\beta}{\mu}\frac{1}{T}\int_T\sum_n \ \{1+\sinh^2\beta\,\mathrm{sech}^2[\beta(n-ut-x_0)]\}\{\mathrm{sech}[\beta(n+1-ut-x_0)]\,\mathrm{sech}[\beta(n-ut-y_0)]\sin(\Delta\sigma-\theta)$$

$$+\mathrm{sech}[\beta(n-1-ut-x_0)]\,\mathrm{sech}[\beta(n-ut-y_0)]\sin(\Delta\sigma+\theta)\}, \tag{79}$$

with the phase difference $\Delta\sigma=\sigma_0-\delta_0$. For vanishing θ and zero phase difference $\Delta\sigma=0$ the single solitons (76) and (77) become standing (stationary) solitons. From expression (79) we infer immediately that then *no energy exchange* between the two strings takes place regardless of the relative soliton positions x_0 and y_0. In particular, the latter fact seems remarkable, recalling that the excitation of an exact two-soliton stationary state of the AL double chain is only possible for opposite solitons of $x_0=y_0$ (see Sec. V). Later we treat the energy exchange numerically.

Using the addition theorems we derive

$$\Delta H_0^{(1)} = -8\alpha\frac{\sinh^2\beta}{\mu}\frac{1}{T}\int_T dt\sum_n \ \frac{1}{\cosh[\beta(n-ut-y_0)]}\left\{\sin\Delta\sigma\cos\theta\frac{\cosh\beta}{\cosh[\beta(n-ut-x_0)]}\right.$$

$$\left.-\cos\Delta\sigma\sin\theta\frac{\sinh\beta\sinh[\beta(n-ut-x_0)]}{\cosh^2[\beta(n-ut-x_0)]}\right\}. \tag{80}$$

In computing the sums in Eq. (80) we note that the arguments of the n-dependent terms are of the form $(n-ut-x_0)$ and $(n-ut-y_0)$. Consequently, the sums in Eq. (80) are invariant under t translations, and thus actually t independent. We then obtain

$$\Delta H_0^{(1)} = -8\alpha\frac{\sinh^2\beta}{\mu}\sum_n \ \frac{1}{\cosh[\beta(n-y_0)]}\left\{\sin\Delta\sigma\cos\theta\frac{\cosh\beta}{\cosh[\beta(n-x_0)]}-\cos\Delta\sigma\sin\theta\frac{\sinh\beta\sinh[\beta(n-x_0)]}{\cosh^2[\beta(n-x_0)]}\right\}. \tag{81}$$
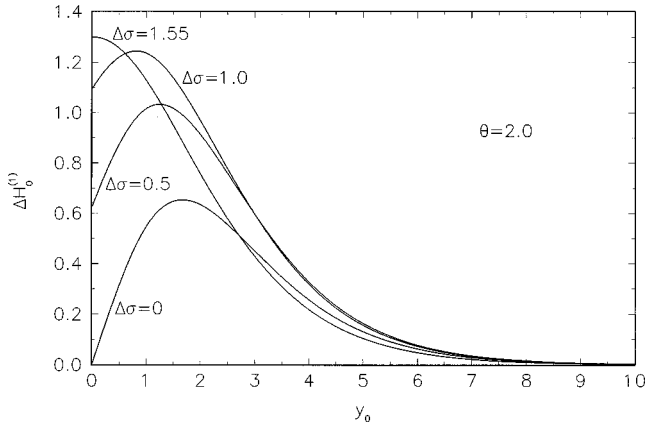
FIG. 6. The energy exchange rate $\Delta H_0^{(1)}$ in dependence on the soliton distance y_0 for $\theta = 2$. We plot the expression for $\Delta H_0^{(1)}$ given in Eq. (81) divided by $-8\alpha \sinh^2 \beta / \mu$. The curve parameter is the phase difference $\Delta \sigma$ as indicated.

Furthermore, for equal soliton positions $x_0 = y_0$ the sums in Eq. (81) are invariant under x_0 translations and thus independent of x_0. Then we assume that, whenever the sum $\sum_{n=-\infty}^{\infty} F(n+x_0)$ does not depend on x_0, it can be converted into an integral [44]

$$\sum_{n=-\infty}^{\infty} F(n+x_0) = \int_{-\infty}^{\infty} dx\, F(x). \tag{82}$$

We obtain

$$\Delta H_0^{(1)} = 16\alpha \frac{\sinh^2 \beta}{\beta \mu} \sin \Delta \sigma \cos \theta \cosh \beta. \tag{83}$$

Apparently, for $\theta = \pm \pi/2$ and/or $\Delta \sigma = 0, \pm \pi$, there is no energy exchange. On the other hand, the maximal energy exchange rate is achieved for $\Delta \sigma = \pm \pi/2$ and $\theta = 0, \pm \pi$.

The general case of $x_0 \neq y_0$ is illustrated in Fig. 6 for $\beta = \text{arccosh}(-1.5)$ and $\theta = -0.2$. We set $x_0 = 0$ and plot $\Delta H_0^{(1)}$ versus y_0 for various values of $\Delta \sigma$, as indicated. Due to the choice $x_0 = 0$ the initial position of the soliton on the upper string is fixed at the site $n = 0$, while the initial position of the soliton on the lower string is moved away from the central lattice site with $y_0 > 0$. In this way y_0 determines the *distance* between the solitons. Interestingly, for undercritical phase differences $\Delta \sigma \lesssim 1.5$ the graphs exhibit an extremum for $y_0 > 0$ corresponding to maximal energy exchange rate. With increased $\Delta \sigma$ the position of the maximum is shifted toward smaller y_0 values. Simultaneously, the energy exchange rate for opposite solitons of $y_0 = 0$ increases. Eventually, for $\Delta \sigma > 1.5$ maximum energy exchange occurs for $y_0 = 0$, and the now monotone curves decay with growing y_0. When θ is varied we obtain similar pictures and the curves are only stretched in the vertical direction. Enhancing β has the effect that the curves decay more rapidly with growing distance y_0. The latter fact becomes plausible by
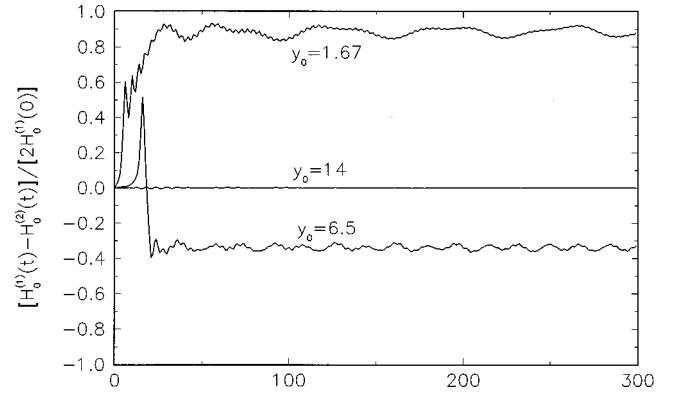
FIG. 7. Temporal behavior of the normed energy difference $[H_0^1(t) - H_0^2(t)]/[2H_0^{(1)}(0)]$ with $H_0^{(1)}(0) = H_0^{(2)}(0)$. Parameters: $\omega = -3$, $\mu = 1$, $V = 1$, and $\alpha = 0.1$. (a) Soliton distance $y_0 = 1.67$ corresponding to maximal energy exchange between the two strings. After a short period of energy migration 90% of the total energy is stored in the upper string. (b) Soliton distance $y_0 = 6.5\%$ and 65% of the total energy becomes stored in the lower string. (c) Soliton distance $y_0 = 14$. Suppressed energy exchange.

noting that the larger θ is the smaller the width of a soliton is, and, hence, their mutual influence diminishes with larger distances y_0.

The different regimes of the energy exchange between the two strings are depicted in Fig. 7. We show the temporal variations of the (normed) energy difference $[H_0^1(t) - H_0^2(t)]/[2H_0^{(1)}(0)]$ with $H_0^{(1)}(0) = H_0^{(2)}(0)$ for three different soliton distances y_0. According to Eq. (81) and Fig. 7, maximal energy exchange between the two strings can be expected for $y_0 = 1.67$. (The main excitation pattern of the exact AL soliton involves five lattice sites.) In fact, after a short transient period of energy migration from the lower string into the upper string the energy difference exhibits small oscillations around the value 0.9, meaning that (approximately) 90% of the total energy is storaged in the upper string. For a wider soliton distance $y_0 = 6.5$ the energy exchange is not as pronounced as for the previous case. Nevertheless, eventually 65% of the total energy become stored in the lower string. For a relative large soliton distance $y_0 = 14$ there is virtually no interaction between the two strings, as seen by the almost negligible variations of the energy difference around zero. We remark that we find good agreement between the energy exchange rate computed analytically on the basis of expression (81) and the numerical results.

Figures 8(a) and 8(b) show, for the soliton distance $y_0 = 1.67$, the amplitude profile of the upper and lower strings, respectively. One clearly sees how the upper chain gains energy at the expense of the lower one. On the upper chain two breathing solitonlike states of distinct amplitudes are created. Whereas the breather of small amplitudes freely propagates along the lattice with a velocity equal to that of an unperturbed soliton, the breather of large amplitude appears to be slow in comparison. The lower chain exhibits a breather having the same velocity as the small amplitude breather on the upper string. For comparison we illustrate in Figs. 9(a) and 9(b) the case of suppressed energy exchange for the large soliton distance $y_0 = 14$. On both strings we observe breathers of equal (maximal and minimal) ampli-
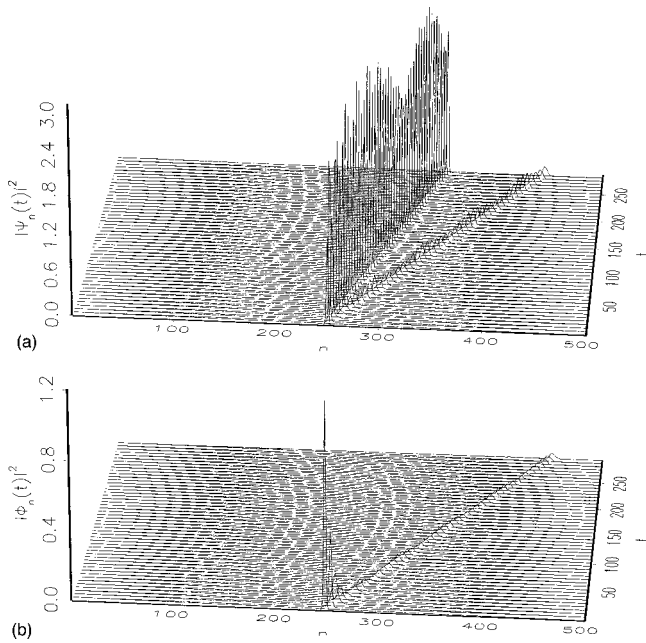
FIG. 8. The amplitude profiles $|\Phi_n(t)|^2$ and $|\Psi_n(t)|^2$ of the upper (a) and lower (b) strings, respectively. Parameters as in Fig. 7(a).

tudes moving along the lattice with unique velocity below the one of an unperturbed soliton.

VII. SUMMARY

In the present paper we investigated the solution behavior of an AL double chain. The first part of the paper dealt with the stationary system belonging to the double chain. We utilized a map approach to describe the stationary states. Interest is focused on the fixed point at the map origin, since for hyperbolic-type stability orbits on the associated invariant manifolds provide bright solitonlike lattice excitations. If the strength of the vertical couplings α exceeds those of the horizontal couplings V the map origin represents a stable elliptic equilibrium. Hence the construction of exact standing solitonlike solutions via homoclinic orbits is then impossible. Furthermore, it is shown that the stationary map is nonintegrable. This is achieved with the help of the Melnikov method assuring transversal intersections of the stable and unstable manifolds of hyperbolic points. The corresponding homoclinic orbit can be used as an initial condition to excite a two-soliton-like *pinned* lattice state. This pinning effect resulting from the nonintegrability of the double chain has to be distinguished from the solution behavior of an isolated one-dimensional AL lattice. The latter is completely integrable. Its stationary solitons derived from the corresponding two-dimensional map can always be moved with any desired velocity through a Galileo boost.

The second part of the paper was devoted to an investigation of the dynamics of the energy exchange between the two (weakly) coupled AL strings. We considered the situation when on both strings an exact AL soliton is initially
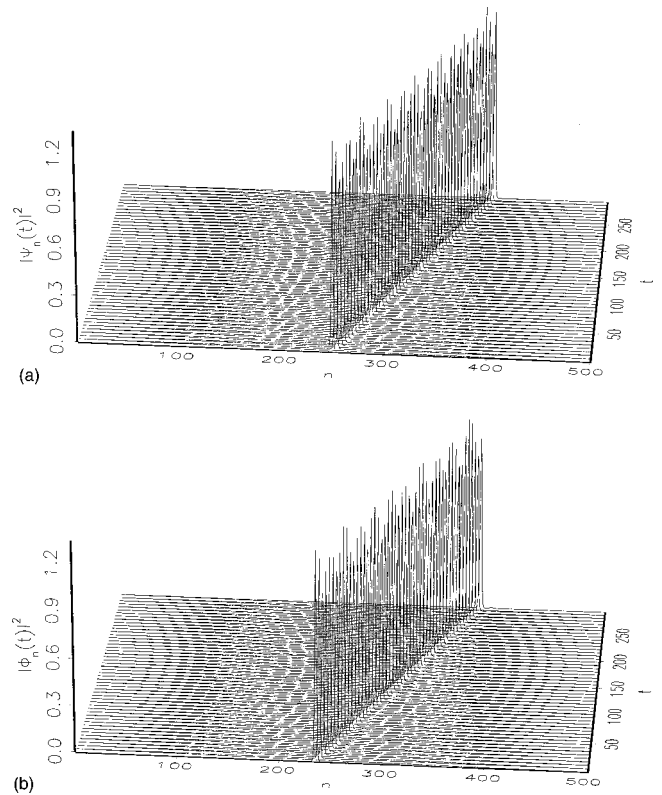
FIG. 9. The amplitude profiles $|\Phi_n(t)|^2$ and $|\Psi_n(t)|^2$ of the upper (a) and lower (b) strings, respectively. Parameters as in Fig. 7(c).

excited. Depending on the initial distance between the solitons as well as their mutual phase relations, there exist distinct energy exchange regimes ranging from suppressed to pronounced exchange. Surprisingly, we found parameter constellations for which maximum energy exchange occurs not for strictly opposite solitons but rather at a certain (nonvanishing) distance between them. As expected, for sufficiently large soliton distances the soliton-soliton interaction vanishes, and energy exchange between the two strings is suppressed. From our studies we conclude that the initial excitation of the single chains with exact AL solitons results in *moving* breathers under the action of the nonintegrable interchain coupling, regardless of the soliton amplitudes as well as their widths. Usually nonintegrability of the lattice system may cause a pinning transition (depending on the soliton parameters [9]) preventing solitonlike solutions or breathers from being moved along the lattice. The only pinned solution we obtained resulted from the homoclinic orbit derived from the stationary system. As an interesting dynamical feature we observe that a single soliton may split into two moving breathing states of different amplitudes as well as different velocities.

[1] A. J. Sievers and S. Takeno, Phys. Rev. Lett. **61**, 970 (1988).

[2] S. Takeno, J. Phys. Soc. Jpn. **58**, 759 (1989).

[3] J. B. Page, Phys. Rev. B **41**, 7835 (1990).

[4] D. K. Campbell and M. Peyrard, in *Chaos*, edited by D. K. Campbell (AIP, New York, 1990).

[5] S. Takeno and K. Hori, J. Phys. Soc. Jpn. **60**, 947 (1991).

[6] K. Hori and S. Takeno, J. Phys. Soc. Jpn. **61**, 2186 (1992).

[7] S. Takeno and S. Homma, J. Phys. Soc. Jpn. **60**, 731 (1991); **62**, 835 (1993); S. Takeno, *ibid.* **61**, 2821 (1992); S. R. Bickham, S. A. Kiselev, and A. J. Sievers, Phys. Rev. B **47**, 14 206 (1993).

[8] K. W. Sandusky, J. B. Page, and K. E. Schmidt, Phys. Rev. B **46**, 6161 (1992).

[9] Ch. Claude, Yu. S. Kivshar, O. Kluth, and K. H. Spatschek, Phys. Rev. B **47**, 14 228 (1992).

[10] T. Dauxois, M. Peyrard, and C. R. Willis, Physica D **57**, 267 (1992); Phys. Rev. E **48**, 4768 (1993); T. Dauxois and M. Peyrard, Phys. Rev. Lett. **70**, 3935 (1993).

[11] Yu. S. Kivshar, Phys. Rev. E **48**, 4132 (1993).

[12] S. Flach, C. R. Willis, and E. Olbrich, Phys. Rev. E **49**, 836 (1994).

[13] S. Flach and C. R. Willis, Phys. Lett. A **181**, 232 (1993); Phys. Rev. Lett. **72**, 1777 (1994).

[14] O. A. Chubykalo, A. S. Kovalev, and O. V. Usatenko, Phys. Lett. A **178**, 129 (1993).

[15] Yu. S. Kivshar and D. K. Campbell, Phys. Rev. E **48**, 3077 (1993).

[16] Yu. S. Kivshar and M. Salerno, Phys. Rev. E **49**, 3543 (1994).

[17] E. W. Laedke, K. H. Spatschek, and S. K. Turitsyn, Phys. Rev. Lett. **73**, 1055 (1994).

[18] S. Aubry, Physica D **86**, 284 (1995).

[19] S. Takeno and M. Peyrard, Physica D **92**, 140 (1996).

[20] G. P. Tsironis and S. Aubry, Phys. Rev. Lett. **77**, 5225 (1996).

[21] D. Chen, S. Aubry, and G. P. Tsironis, Phys. Rev. Lett. **77**, 4776 (1996).

[22] A. B. Aceves, C. De Angelis, T. Peschel, R. Muschall, F. Lederer, S. Trillo, and S. Wabnitz, Phys. Rev. E **53**, 1172 (1996).

[23] J. L. Marin and S. Aubry, Nonlinearity **9**, 1501 (1996).

[24] T. Cretegny and S. Aubry, Phys. Rev. B **55**, 11 929 (1997).

[25] S. Flach and C. R. Willis, Phys. Rep. **295**, 181 (1998).

[26] R. S. MacKay and S. Aubry, Nonlinearity **7**, 1623 (1994).

[27] D. Bambusi, Nonlinearity **9**, 433 (1996).

[28] P. Marquié, J. M. Bilbault, and M. Remoissenet, Phys. Rev. E **51**, 6127 (1995).

[29] S. V. Manakov, Sov. Phys. JETP **38**, 248 (1974).

[30] V. E. Zakharov and E. I. Schulman, Physica D **4**, 270 (1982).

[31] S. G. Evangelides, L. F. Moldenhauer, J. P. Gordon, and N. S. Bergano, J. Lightwave Technol. **10**, 28 (1992).

[32] N. Akhmediev and J. M. Soto-Crespo, Phys. Rev. E **49**, 5742 (1994).

[33] M. Peyrard and A.R. Bishop, Phys. Rev. Lett. **62**, 2755 (1989).

[34] K. Forinash, A. R. Bishop, and P. S. Lomdahl, Phys. Rev. B **43**, 10 743 (1991).

[35] K. Forinash and J. Keeney, J. Phys. A **25**, 6087 (1992).

[36] L. D. Faddeev and L. A. Takhtajan, *Hamiltonian Methods in the Theory of Solitons* (Springer-Verlag, Berlin, 1987).

[37] M. J. Ablowitz and P. A. Clarkson, *Solitons, Nonlinear Evolution Equations and Inverse Scattering* (Cambridge University Press, New York, 1991).

[38] M. J. Ablowitz and J. F. Ladik, J. Math. Phys. **17**, 1011 (1976).

[39] B. M. Herbst and M. J. Ablowitz, Phys. Rev. Lett. **62**, 2065 (1989).

[40] A. R. Bishop, M. G. Forest, D. W. McLaughlin, and E. A. Overmann, Phys. Lett. A **144**, 17 (1990).

[41] A. R. Bishop, R. Flesch, M. G. Forest, D. W. McLaughlin, and E. A. Overmann, SIAM (Soc. Ind. Appl. Math.) J. Math. Anal. **21**, 1511 (1990).

[42] R. Scharf and A. R. Bishop, Phys. Rev. A **43**, 6535 (1991).

[43] M. Salerno, Phys. Rev. A **46**, 6856 (1992).

[44] D. Cai, A. R. Bishop, and N. Grønbech-Jensen, Phys. Rev. Lett. **72**, 591 (1994).

[45] V. V. Konotop, O. A. Chubykalo, and L. Vázquez, Phys. Rev. E **48**, 563 (1993).

[46] D. Cai, A.R. Bishop, N. Grønbech-Jensen, and M. Salerno, Phys. Rev. Lett. **74**, 1186 (1995); D. Cai, A. R. Bishop, and N. Grønbech-Jensen, Phys. Rev. E **52**, 5784 (1995); **53**, 1202 (1996).

[47] D. Hennig, K. Ø. Rasmussen, H. Gabriel, and A. Bülow, Phys. Rev. E **54**, 5788 (1996).

[48] J. E. Howard and R. S. MacKay, Phys. Lett. A **122**, 331 (1987).

[49] A. J. Lichtenberg and M. A. Liebermann, *Regular and Stochastic motion* (Springer-Verlag, New York, 1992).

[50] S. Wiggins, *Global Bifurcations and Chaos—Analytical Methods* (Springer-Verlag, New York, 1988).

[51] V. K. Melnikov, Trans. Moscow Math. Soc. **12**, 1 (1963).

[52] M. L. Glasser, V. Papageorgiou, and T. Bountis, SIAM (Soc. Ind. Appl. Math.) J. Appl. Math. **49**, 692 (1989).

[53] S. N. Chow and M. Yamashita, in *Nonlinear Equations in the Applied Sciences* (Academic, New York, 1992).

[54] J. K. Palmer, J. Diff. Eqns. **55**, 225 (1984).

[55] S. N. Chow, K. K. Hale, and J. Mallet-Paret, J. Diff. Eqns. **37**, 351 (1980).

[56] T. Bountis, A. Goriely, and M. Kollmann, Phys. Lett. A **206**, 38 (1995).

[57] P. F. Byrd and M. D. Friedman, *Handbook of Elliptic Integrals for Engineers and Scientists* (Springer-Verlag, New York, 1971).